

# Signals With or Without Wires in Modern Detectors

by

Julie Helen Wyatt

Submitted to the Department of Physics  
in partial fulfillment of the requirements for the degree of

Bachelor of Science in Physics

at the

MASSACHUSETTS INSTITUTE OF TECHNOLOGY

June 2001

© Julie Helen Wyatt, MMI. All rights reserved.

The author hereby grants to MIT permission to reproduce and  
distribute publicly paper and electronic copies of this thesis document  
in whole or in part.

Author .....  
Department of Physics  
May 8, 2001

Certified by .....  
Ulrich Becker  
Professor  
Thesis Supervisor

Accepted by .....  
David E. Pritchard  
Chairman, Department Committee on Graduate Students



# Signals With or Without Wires in Modern Detectors

by

Julie Helen Wyatt

Submitted to the Department of Physics  
on May 8, 2001, in partial fulfillment of the  
requirements for the degree of  
Bachelor of Science in Physics

## Abstract

Conventional gaseous particle detectors use wires for signal formation and detection. Electrons drift toward the wire and undergo amplification in the electric field near the wire. Wire detectors are fragile and suffer problems with aging, however, so new technology is being developed. This thesis studies conventional wire detectors, to understand the parameters involved for application to a stable detector. It proceeds to study wireless detectors in the study of the very new Gas Electron Multiplier (GEM). GEM foils are made of copper clad Kapton foil with an array of evenly spaced holes (typically  $80 \mu m$ ). The GEM foils generate high fields through the holes by applying a potential difference across the upper and lower surfaces. They are also less fragile and less prone to aging. This could be particularly useful for the large scale particle detectors and for space experiments.

Thesis Supervisor: Ulrich Becker

Title: Professor

## Acknowledgments

The author would like to acknowledge Professors Ulrich Becker, Peter Fisher, and Kate Scholberg for guidance as well as Evan Fortunato, Jesse Kirchner, Rafael Dinner, Jesse Wodin, Bilge Demirköz, Reyco Henning, Ben Monreal, Gianpaolo Carosi, Bernard Asare, and Eileen Kelly for support.

# Contents

<b>1</b>	<b>Introduction</b>	<b>11</b>
1.1	Gas Amplification . . . . .	11
1.2	Pulse Formation . . . . .	12
1.3	Cylindrical Proportional Chamber . . . . .	12
1.4	Gas Electron Multiplier . . . . .	15
<b>2</b>	<b>Wire Amplification Measurements</b>	<b>17</b>
2.1	Apparatus . . . . .	17
2.2	Measurements . . . . .	18
2.2.1	Voltage Dependence . . . . .	20
2.2.2	Pressure Dependence . . . . .	21
2.2.3	Stability . . . . .	23
<b>3</b>	<b>GEM Amplification Measurements</b>	<b>29</b>
3.1	Apparatus . . . . .	29
3.1.1	GEM Foils . . . . .	29
3.1.2	Chamber Construction . . . . .	30
3.1.3	First GEM Experiment . . . . .	31
3.2	Measurements . . . . .	32
3.2.1	Measurements . . . . .	33
3.2.2	Single GEM . . . . .	36
3.2.3	Double GEM . . . . .	41



# List of Figures

1-1	Geometry of GEM hole. . . . .	15
2-1	Setup for drift tubes. . . . .	18
2-2	Gas system for drift tubes. . . . .	18
2-3	Pulse height distribution from $\text{Fe}^{55}$ in $\text{Xe}:\text{CO}_2$ . . . . .	19
2-4	Measurements Gain v. Voltage for Ne with and $\text{Fe}^{55}$ source. . . . .	20
2-5	Measurements Gain v. Voltage for Ar with and $\text{Fe}^{55}$ source. . . . .	21
2-6	Measurements Gain v. Voltage for Kr with and $\text{Fe}^{55}$ source. . . . .	23
2-7	Measurements Gain v. Voltage for Xe with and $\text{Fe}^{55}$ source. . . . .	24
2-8	Measurements Gain v. Pressure for Ar with and $\text{Fe}^{55}$ source. . . . .	25
2-9	Measurements Gain v. Pressure for Ar with and $\text{Fe}^{55}$ source. . . . .	26
2-10	Measurements Gain v. Pressure for Ar with and $\text{Fe}^{55}$ source. . . . .	26
2-11	Setup time. . . . .	27
2-12	Stability Measurements. . . . .	28
2-13	Long term stability. . . . .	28
3-1	a) Medium GEM foil illuminated from below and b) from above. . . . .	30
3-2	a) Medium GEM foil with grating, holes are in focus. b) Same foil, but grating is in focus. . . . .	31
3-3	Gem stretched on Aluminum ring. . . . .	32
3-4	Gem foil mounted on G10 frame. . . . .	33
3-5	Schematic Diagrams for a) GEM chamber and b) wire circuit. . . . .	34
3-6	Circuit connecting GEM foil. . . . .	34
3-7	Assembled chamber complete with circuit elements. . . . .	34

3-8	a) GEM foil with large holes illuminated from above and b) with grating.	35
3-9	GEM chamber schematic for a single foil. . . . .	36
3-10	Signal charge distribution from a $5.9keV\gamma$ ionization in P10. The peak at channel $-330$ corresponds to the calibration signals with $V_{wire} = 1600V$ . The other peaks are gradually GEM amplified signals. . . . .	37
3-11	Signal charge distribution from a $5.9keV\gamma$ ionization in P10. The peak at channel $-330$ corresponds to the calibration signals with $V_{wire} = 1600V$ . The GEM amplified signals (near channel $-1400$ ) show little dependence on the drift field in volume $d$ . . . . .	38
3-12	Signal v. Gem Voltage for Single GEM chamber. . . . .	39
3-13	Signal v. Cathode Voltage for Single GEM chamber. . . . .	40
3-14	Circuit connecting two GEM foils. . . . .	41
3-15	Pulse height for double GEM v. $V_{G1} = V_{G2}$ . . . . .	42



# List of Tables

2.1	Gas Mixtures Studied . . . . .	19
2.2	Measured values for $\frac{1}{G} \frac{\partial G}{\partial V}$ in three gain regions in % per Volt. . . . .	22
2.3	Measured values for $\frac{1}{G} \frac{\partial G}{\partial P}$ in three gain regions in % per mbar. . . . .	22
2.4	Measurements of Diethorn Parameters in Noble Gases . . . . .	27



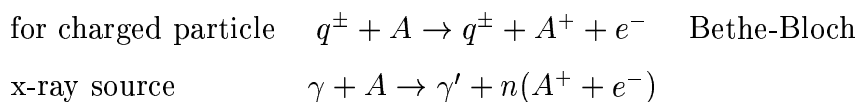
# Chapter 1

## Introduction

### 1.1 Gas Amplification

Multi-wire proportional chambers and drift chambers play a dominating role in particle detection. To better understand these types of detectors, we have studied the amplification of ionization of gas molecules along particle tracks for detectors operating in the proportional region, i.e. the region in which the amplification signal is proportional to the primary ionization. A high energy particle's energy loss through the gas is described by the Bethe-Bloch formula [3], and typically creates 80 electron-ion pairs per centimeter in Argon for a minimum ionizing particle. Amplification of the initial ionization occurs due to the fact that electrons, traveling over a mean free path, under the influence of an electric field, gain energy greater than the ionization potential of the gas atoms. This amplification is an avalanche, thus it is very sensitive to changes in the electric field, the gas pressure, and the gas mixture.

In general, there are two processes which occur in ionization caused by a radiation in a detector. There are the primary ionization clusters, which are caused by the particle itself ionizing gas atoms (with knock on electrons causing more ionization),



creating electron-ion pairs. The signal, however, is produced by the amplification ionizations occurring close to a wire or in the hole of a GEM,



If  $n$  is the number of electrons created in the avalanching process,

$$dn = \alpha n dx, \quad (1.2)$$

where  $\alpha$  is the First Townsend coefficient, and  $x$  is the distance traveled. Thus, the multiplication factor, the gain of the detector, is [2]

$$G = \frac{n}{n_o} = e^{\alpha(E)x}, \quad (1.3)$$

with  $\alpha(E)$  given in [2].

## 1.2 Pulse Formation

Whereas the arriving electrons give a small and brief negative pulse, the bulk of the signal is formed by the mirror charges of the positive ions from the avalanche on the wire [2]. The ions drift causing a change of mirror charges giving rise to a current

$$I = \frac{dQ}{dt}, \quad (1.4)$$

on the wire. The pulse has a fast rise time from the time where the electrons are reaching the wire. The ion mobility is approximately a factor of 1000 slower, and comprises the long tail in accordance with the positive ions moving away.

## 1.3 Cylindrical Proportional Chamber

The gain at the proportional wire can be obtained by integrating Equation 1.2 over the path between  $s_{min}$ , the point at which the field is high enough to start an

avalanche, to the diameter of the wire,  $a$ . This yields [2]

$$\frac{n}{n_0} = \exp \int_{s_{min}}^a \alpha(s) ds = \exp \int_{E_{min}}^{E(a)} \frac{\alpha(E)}{\frac{dE}{ds}} dE, \quad (1.5)$$

where  $\frac{dE}{ds}$  is the electric field gradient, which is equivalent to  $-\frac{dE}{dr}$ ,  $E(a)$  is the field at the wire, and  $E_{min}$  is the minimum electric field needed for an electron to pick up, in a mean free path, enough energy for secondary ionizations. For a cylindrical geometry of a proportional drift tube, the electric field is

$$E(r) = \frac{V}{\ln\left(\frac{b}{a}\right) r}, \quad (1.6)$$

where  $V$  is the potential of the wire,  $b$  is the inner radius of the tube, and  $a$  is the wire radius. This yields an electric field gradient in the direction of the wire of

$$\frac{dE}{dr} = \frac{V}{\ln\left(\frac{b}{a}\right) r^2} = \frac{\ln\left(\frac{b}{a}\right) E^2}{V}. \quad (1.7)$$

Substituting this into Equation 1.5, we get

$$\frac{n}{n_0} = \exp \int_{E_{min}}^{E(a)} \frac{V \alpha(E)}{\ln\left(\frac{b}{a}\right) E^2} dE = G. \quad (1.8)$$

Diethorn [1] made the approximation in the presence of an operational field  $E$ ,

$$\alpha(E) \approx \beta E. \quad (1.9)$$

Substituting into Equation 1.8, we get

$$G = \exp \int_{E_{min}}^{E(a)} \frac{V \beta}{\ln\left(\frac{b}{a}\right) E} dE. \quad (1.10)$$

Integrating this function and substituting Equation 1.6 for  $E(a)$ , the field at the wire, yields

$$\ln G = \frac{\beta V}{\ln\left(\frac{b}{a}\right)} \ln \frac{V}{\ln\left(\frac{b}{a}\right) a E_{min}}. \quad (1.11)$$

Since the gain can be expressed in terms of one parameter,  $\alpha(E)$ , approximated by  $\beta E$ ,  $\beta$  must be related to the energy required to release an additional electron from the gas. A relation for this can be obtained by looking at the potential energy difference along the path of the electrons forming the avalanche. This difference is given by

$$\Phi(a) - \Phi(s_{min}) = \int_a^{s_{min}} E(r) dr = \frac{V}{\ln(\frac{b}{a})} \ln \frac{V}{\ln(\frac{b}{a}) a E_{min}}. \quad (1.12)$$

With this energy, there can be  $Z$  generations, each doubling the number of electrons.

$$Z = \frac{[\Phi(a) - \Phi(s_{min})]}{\Delta V}, \quad (1.13)$$

if  $\Delta V$  is the effective ionization potential of the gas. The effective ionization potential must be larger than the actual ionization potential of the gas, because it includes inelastic collisions which do not result in ionizations.  $Z$  generations give a gain factor of

$$G = 2^Z. \quad (1.14)$$

Now there are two relations for the gain (Equations 1.11 and 1.14) which can be equated, and  $\beta$  can be rewritten in terms of known quantities. Rewriting Equation 1.14, we have

$$\ln G = Z \ln 2 = \frac{\ln 2}{\Delta V} \frac{V}{\ln(\frac{b}{a})} \ln \frac{V}{\ln(\frac{b}{a}) a E_{min}} \quad (1.15)$$

Since the start of the avalanche must be a function of the mean free path,  $\lambda$ , of the gas, which, in turn, is related to the gas density,  $\rho$ , i.e.

$$E_{min}(\rho) = E_{min}(\rho_0) \frac{\rho}{\rho_0} \quad (1.16)$$

Combining Equation 1.15 with our earlier expression for the gain (Equation 1.11) along with the rewriting of  $E_{min}$ , we arrive at the Diethorn [1] formula:

$$\ln G = \frac{V \ln 2}{\ln\left(\frac{b}{a}\right) \Delta V} \ln \left[ \frac{V}{\ln\left(\frac{b}{a}\right) a E_{min}(\rho) \left(\frac{\rho}{\rho_0}\right)} \right], \quad (1.17)$$

which is an expression relating the gain to parameters of the gas,  $E_{min}$  and  $\Delta V$ . These are microscopic properties of the gas which can be extracted from measurements of the gain.

## 1.4 Gas Electron Multiplier

A Gas Electron Multiplier (GEM) is made of an insulating layer of kapton foil with copper coating on both sides, with many equally spaced holes etched through. The amplification caused by the GEM is due to the high electric fields through the holes which can be obtained by putting a potential across the copper coatings.

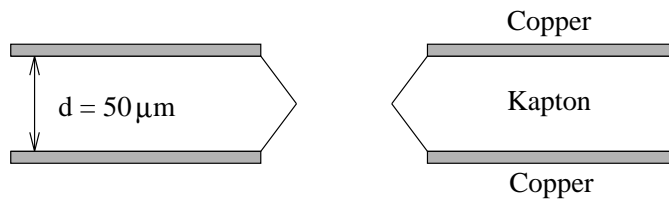


Figure 1-1: Geometry of GEM hole.

The geometry of the GEM foil is shown in Figure 1-1. A rough estimate of the electric field through the holes is

$$E \approx \frac{V_{GEM}}{d} \approx \frac{300V}{50\mu m} \approx 60kV/cm \quad (1.18)$$

where  $V_{GEM}$  is the voltage across the GEM foil and  $d$  is the thickness of the foil, in this case  $50\mu m$ . The electron must reach the corresponding  $E_{min}$  point (as derived in the previous section) for the GEM foil before amplification can occur. A typical value for  $E_{min}$  is  $40kV/cm$ . Whereas the field must be calculated by a program like Maxwell [5], we assume that  $E > 40kV/cm$  over about  $40\mu m$  through the hole.

The gain depends on the mean free path of the gas,  $\lambda$ , given by [4]

$$\lambda = \frac{1}{\sqrt{2}} \frac{kt}{\sigma_0 P}, \quad (1.19)$$

where  $\sigma_0$  is the total cross section for a collision, and  $P$  is the pressure. Typically, this is about  $5\mu m$ , yielding  $Z = \frac{40\mu m}{5\mu m}$  generations and a gain of

$$G = 2^Z = 256, \quad (1.20)$$

in this case. Assuming that  $Z$  is proportional to the  $V_{GEM}$ , we expect exponential behavior of gain on voltage.



# Chapter 2

## Wire Amplification Measurements

The gas multiplication for Ne, Ar, Kr, and Xe with hydrocarbon quenchers was measured in proportional tubes of cylindrical geometry. The systematic study of the avalanche multiplication provides future chamber designers with data concerning the effects of changes in pressure and voltage on the gain as well as absolute gain calibrations.

Studies such as these are needed for proportional chambers which cannot optimize signal and drift fields simultaneously. Variations in pressure and voltage are studied and measurements of differential and absolute gain are presented.

### 2.1 Apparatus

The apparatus is shown in Figures 2-1 and 2-2. The detector consists of a drift tube with a 30  $\mu\text{m}$  gold plated tungsten wire at positive high voltage. The signal is coupled through a 1 nF capacitor to the preamplifier, and then fed through the main amplifier. The amplifier output is split with a T-connector, one side going to the discriminator, the other to the ADC. The first signal is used to generate a gate of several microseconds, the second is attenuated to match the ADC range. The ADC requires a gate of 2  $\mu\text{s}$ , which is generated by the discriminator triggering a pulse generator. The ADC modules in the CAMAC crate are read out by a controller into a PC running LabWindows, a data acquisition coding environment. Signal heights

are then histogrammed and analyzed.

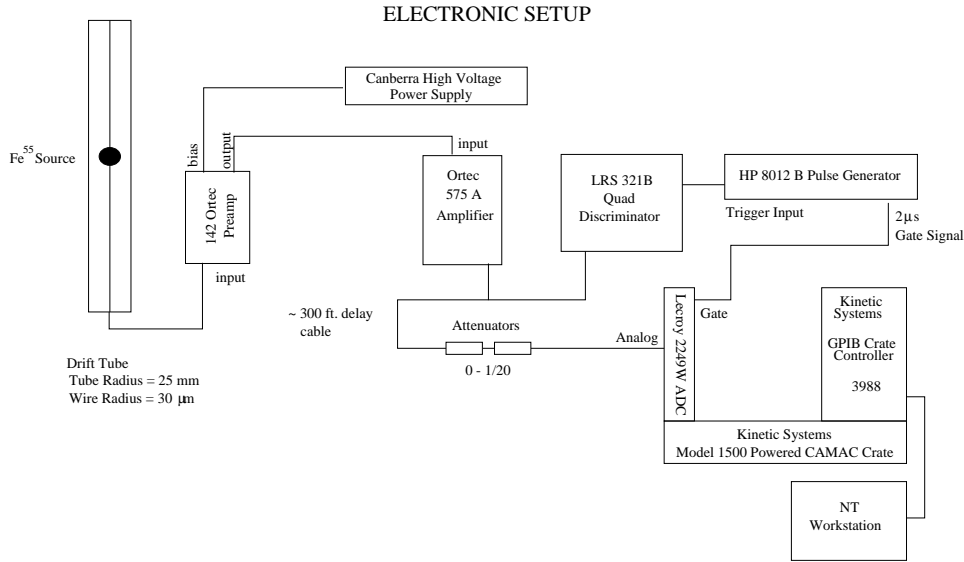


Figure 2-1: Setup for drift tubes.

Figure 2-2 shows the gas system for the drift tube. The pressure changes of  $\pm 25\text{mbar}$  are generated by flowing the gas through tubes which differ in length by 25 cm of water column.

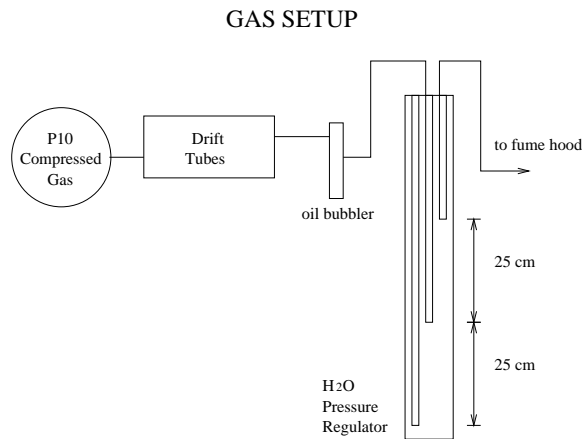


Figure 2-2: Gas system for drift tubes.

## 2.2 Measurements

Noble gases with hydrocarbon quenchers are studied (see Table 2.1) through differential measurements consisting of  $\pm 25\text{V}$  variations in voltage and  $\pm 25\text{mbar}$  in pressure

Table 2.1: Gas Mixtures Studied

	Ne	Ar	Kr	Xe
CH <sub>4</sub>	90:10 70:30	90:10	90:10 80:20 70:30 60:40	90:10 70:30
C <sub>2</sub> H <sub>6</sub>	90:10 70:30	90:10	90:10	90:10 70:30
CF <sub>4</sub>				90:10 80:20
CO <sub>2</sub>				80:20

around three operational points in the range of  $10^3 < G < 10^5$ .

Figure 2-3 shows a typical Fe<sup>55</sup> spectrum in Xe:CO<sub>2</sub>(80:20). This is the histogram of unnormalized charge, centered at ADC channel 1000, from ionization generated by a 5.9 keV  $\gamma$ . The channel for the gain is defined to be the mean of a Gaussian fit to the peak, with the absolute gain factor is then determined by the system calibration. For the gain measurements given below, we assume 200 ionization electrons from a stopped 5.9keV  $\gamma$ , regardless of the gas.

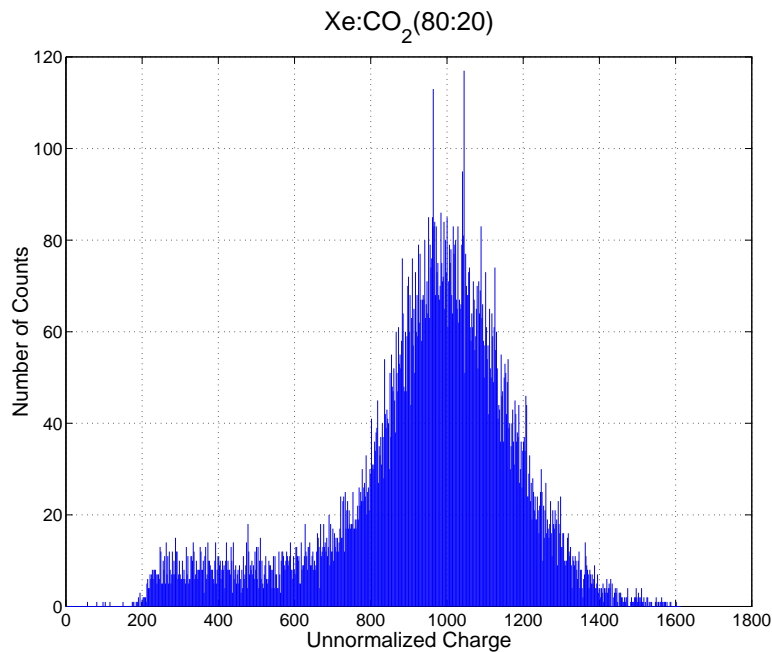


Figure 2-3: Pulse height distribution from Fe<sup>55</sup> in Xe:CO<sub>2</sub>.

## 2.2.1 Voltage Dependence

Measurements of the voltage dependence of the gain are presented in Figures 2-4, 2-5, 2-6, and 2-7. The data exhibit exponential behavior in gain with respect to changes in voltage. Repeated measurements show the effects of small changes in voltage and the degree of reproducibility.

Comparing quenchers, trends can be seen independent of the noble gas used. Mixtures using Methane require more voltage to achieve the same gain as compared to those using Ethane. The Ne (Fig 2-4) data have steeper slopes than the other noble gas mixtures. Also, the gain is reached at relatively lower voltages. Kr requires higher voltages and shows flatter slopes than Ne or Ar. This effect is even more pronounced in the Xe measurements.

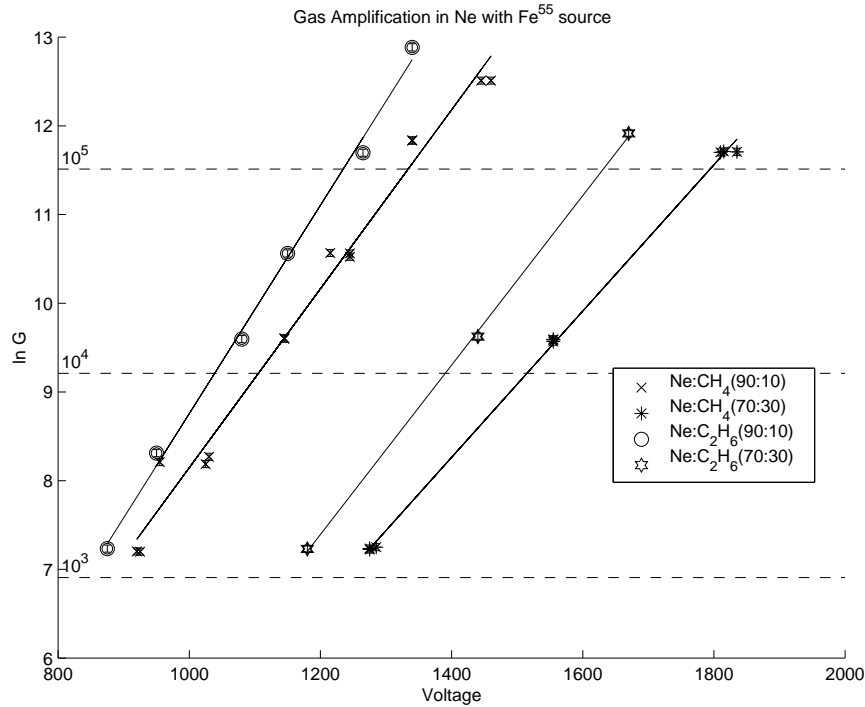


Figure 2-4: Measurements Gain v. Voltage for Ne with and Fe<sup>55</sup> source.

Typical values for  $\frac{1}{G} \frac{\partial G}{\partial V}$  are given in Table 2.2.

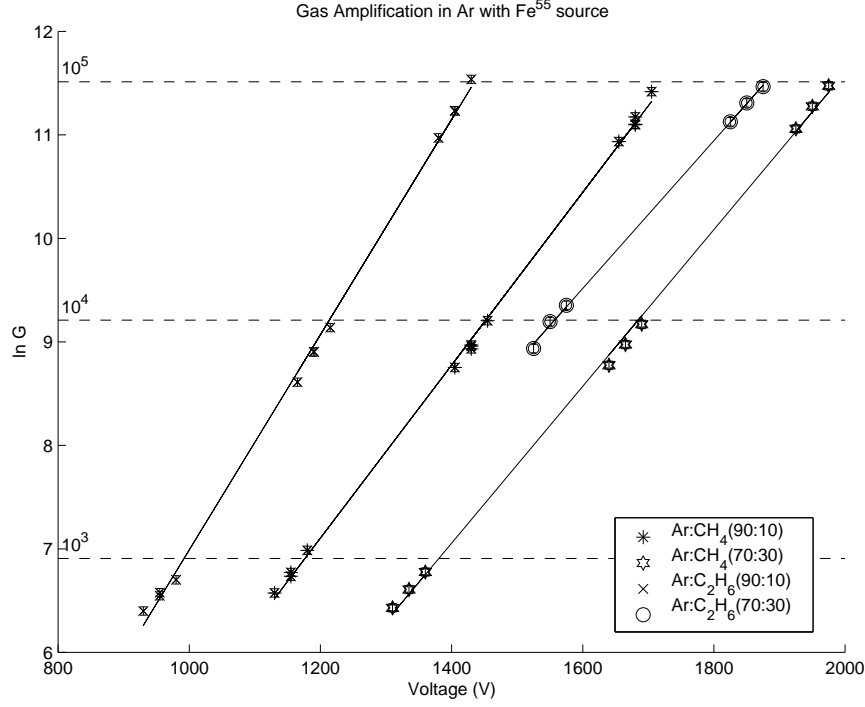


Figure 2-5: Measurements Gain v. Voltage for Ar with and  $\text{Fe}^{55}$  source.

## 2.2.2 Pressure Dependence

Pressure measurements using  $\pm 25$  mbar variations around 1050 mbar are presented for Ar quenched with Ethane and Methane (see Figures 2-8, 2-9, 2-10) in three different amplification regions.

Pressure measurements can be used, along with voltage dependence measurements to extract the Diethorn parameters,  $E_{min}$  and  $\Delta V$ , from measurements of gas amplification. The parameters can be isolated by taking derivatives of the Diethorn formula (Equation 1.17), i.e. [2]

$$\frac{dG}{G} = -\frac{V \ln 2}{\Delta V \ln\left(\frac{b}{a}\right) \rho} \frac{d\rho}{\rho}, \quad (2.1)$$

yielding an expression for  $\Delta V$  to be

$$\Delta V = -\frac{1}{\frac{1}{G} \frac{dG}{d\rho}} \frac{V \ln 2}{\Delta V \ln\left(\frac{b}{a}\right) \rho}. \quad (2.2)$$

Measurements of  $E_{min}$  and  $\Delta V$  are given in Table 2.4.

Table 2.2: Measured values for  $\frac{1}{G} \frac{\partial G}{\partial V}$  in three gain regions in % per Volt.

GAS	%	$\approx 10^3$	$G \approx 10^4$	$G \approx 10^5$
Ne:CH <sub>4</sub>	(90 : 10)	0.974 ± 0.050	1.1040 ± 0.055	1.206 ± 0.050
Ne:CH <sub>4</sub>	(70 : 30)	0.788 ± 0.056	0.846 ± 0.048	0.868 ± 0.047
Ne:C <sub>2</sub> H <sub>6</sub>	(90 : 10)	1.061 ± 0.076	1.193 ± 0.089	1.252 ± 0.090
Ne:C <sub>2</sub> H <sub>6</sub>	(70 : 30)	0.929 ± 0.050	0.973 ± 0.047	0.906 ± 0.051
Ar:CH <sub>4</sub>	(90 : 10)	0.830 ± 0.037	0.915 ± 0.039	1.136 ± 0.050
Ar:CH <sub>4</sub>	(70 : 30)	0.798 ± 0.037	0.833 ± 0.037	0.846 ± 0.040
Ar:C <sub>2</sub> H <sub>6</sub>	(90 : 10)	0.605 ± 0.049	1.102 ± 0.047	1.136 ± 0.050
Ar:C <sub>2</sub> H <sub>6</sub>	(70 : 30)		0.684 ± 0.037	0.833 ± 0.037
Kr:CH <sub>4</sub>	(90 : 10)	0.794 ± 0.045	0.800 ± 0.034	0.657 ± 0.038
Kr:CH <sub>4</sub>	(80 : 20)	0.738 ± 0.049	0.798 ± 0.042	0.646 ± 0.045
Kr:CH <sub>4</sub>	(70 : 30)	0.720 ± 0.046	0.733 ± 0.039	0.695 ± 0.048
Kr:CH <sub>4</sub>	(60 : 40)	0.654 ± 0.044	0.699 ± 0.042	0.663 ± 0.039
Kr:C <sub>2</sub> H <sub>6</sub>	(90 : 10)	0.842 ± 0.046	0.870 ± 0.047	0.804 ± 0.046
Xe:CO <sub>2</sub>	(80 : 20)	0.713 ± 0.035	0.694 ± 0.040	
Xe:CF <sub>4</sub>	(90 : 10)	0.828 ± 0.028		
Xe:CF <sub>4</sub>	(80 : 20)	0.767 ± 0.042	0.794 ± 0.040	

Table 2.3: Measured values for  $\frac{1}{G} \frac{\partial G}{\partial P}$  in three gain regions in % per mbar.

GAS	%	$G \approx 10^3$	$G \approx 10^4$	$G \approx 10^5$
Ne:CH <sub>4</sub>	(90 : 10)	-0.248 ± 0.039	-0.320 ± 0.044	-0.441 ± 0.042
Ne:CH <sub>4</sub>	(70 : 30)	-0.359 ± 0.052	-0.386 ± 0.043	-0.458 ± 0.043
Ne:C <sub>2</sub> H <sub>6</sub>	(90 : 10)	-0.283 ± 0.060	-0.326 ± 0.034	-0.431 ± 0.053
Ne:C <sub>2</sub> H <sub>6</sub>	(70 : 30)	-0.358 ± 0.046	-0.424 ± 0.050	-0.490 ± 0.057
Ar:CH <sub>4</sub>	(90 : 10)	-0.358 ± 0.033	-0.464 ± 0.032	-0.487 ± 0.0430
Ar:CH <sub>4</sub>	(70 : 30)	-0.497 ± 0.033	-0.507 ± 0.028	-0.561 ± 0.037
Ar:C <sub>2</sub> H <sub>6</sub>	(90 : 10)	-0.353 ± 0.050	-0.370 ± 0.039	-0.487 ± 0.043
Ar:C <sub>2</sub> H <sub>6</sub>	(70 : 30)		-0.484 ± 0.029	-0.497 ± 0.033
Kr:CH <sub>4</sub>	(90 : 10)	-0.441 ± 0.047	-0.435 ± 0.033	-0.456 ± 0.035
Kr:CH <sub>4</sub>	(80 : 20)	-0.444 ± 0.044	-0.494 ± 0.036	-0.383 ± 0.043
Kr:CH <sub>4</sub>	(70 : 30)	-0.496 ± 0.043	-0.520 ± 0.037	-0.493 ± 0.045
Kr:CH <sub>4</sub>	(60 : 40)	-0.462 ± 0.043	-0.532 ± 0.043	-0.496 ± 0.030
Kr:C <sub>2</sub> H <sub>6</sub>	(90 : 10)	-0.409 ± 0.047	-0.434 ± 0.046	-0.425 ± 0.041
Xe:CO <sub>2</sub>	(80 : 20)	-0.462 ± 0.038	-0.541 ± 0.037	
Xe:CF <sub>4</sub>	(90 : 10)	-0.461 ± 0.026		
Xe:CF <sub>4</sub>	(80 : 20)	-0.586 ± 0.036	-0.525 ± 0.038	

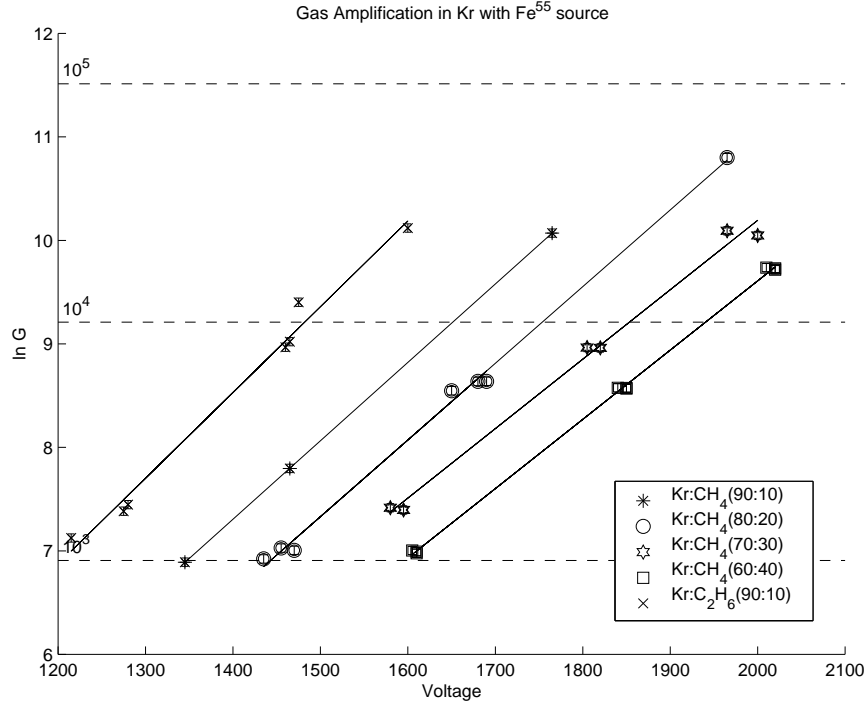


Figure 2-6: Measurements Gain v. Voltage for Kr with and Fe<sup>55</sup> source.

Exact knowledge of pressure dependence is necessary for calorimeters, where the hadron energy  $E \propto \Sigma$  signal heights. For example, a calorimeter calibrated at Brookhaven ( 1000 mbar) gave a 30% higher reading at CERN ( 940 mbar). Our measurements provide the conversion for data and the Diethorn formula can be used for an analytical description for extrapolations which are not too large. However, fitting  $\Delta V$  and  $E_{min}$  simultaneously yields strong correlations of the values. Therefore, in the future, we will use a wider range in  $P$  and Equation 2.2 to determine  $\Delta V$  first and use the voltage dependence to obtain stable values of  $E_{min}$  thereafter.

### 2.2.3 Stability

As the gain measurements are exponentially sensitive to variations in voltage, pressure, and gas purity, calibrations and tests for system stability must be performed periodically. The tests are all done with P10 at 1155 V, with an expected gain factor of  $5 * 10^3$ . All data has been normalized to 25 °C and 1050 mbar.

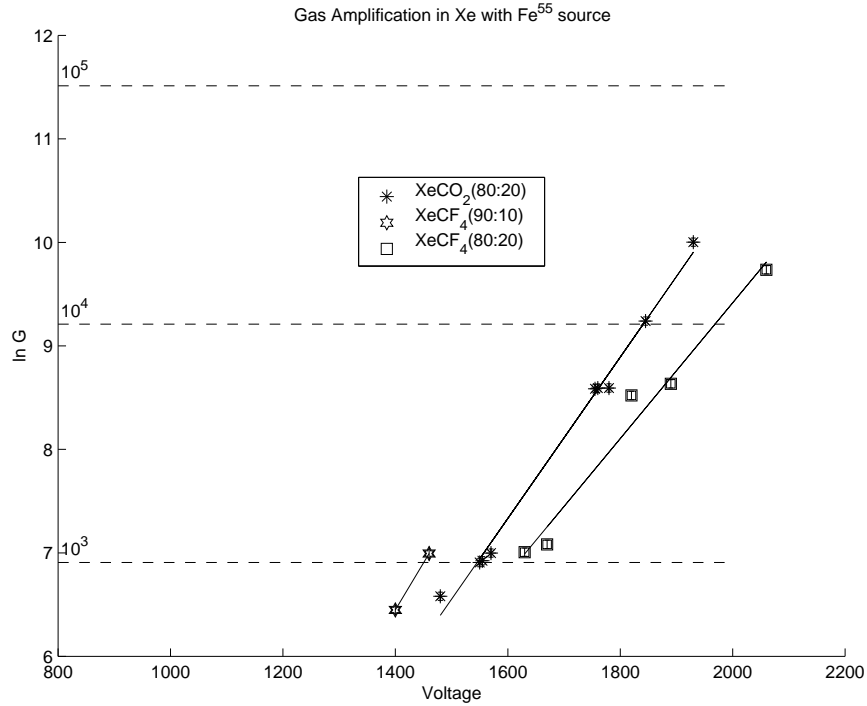


Figure 2-7: Measurements Gain v. Voltage for Xe with and Fe<sup>55</sup> source.

### Gas Purity: Setup Time

The system was first flushed with air. The P10 was turned on and flowed at a steady rate, while data was taken every five minutes. The flow rate was estimated using a weather balloon and finding its volume. The volume labeled on the plots is the result of this rough estimate. As seen in Figure 2-11, the system is stable to  $\pm 2\%$  for  $> 20$  volume exchanges after being exposed to air.

### Gas Purity Between Measurements and Electronic Stability

The focus of test two is to look at short term stability for the experiment to determine the setup time between measurements done on the same gas. The time is one day later than the previous test. The gas has been off and the electronics have been left on. Figure 2-12(a) shows the system to be stable after  $> 10$  volumes flushed.

The test for electronic stability is done by leaving the electronics off but allowing the gas to keep flushing. The beginning of the test is when the electronics are turned on again. As seen in Figure 2-12(b), there is little 'warm up' drift due to the



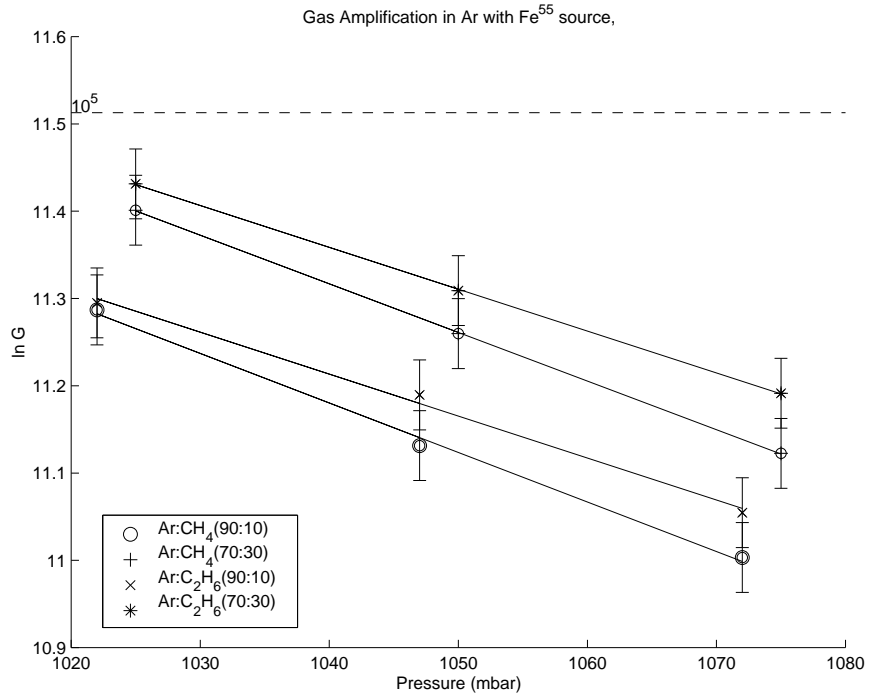


Figure 2-8: Measurements Gain v. Pressure for Ar with and  $Fe^{55}$  source.

electronics, and the system is stable after the time it takes to flush 4 gas volumes.

### Long Term Stability and Setup

Measurements (Fig. 2-13) have been taken with other gases since the previous result. P10 must be newly flushed through the system resulting in a setup time. Note that the long term results yield a higher mean channel number. This gives an estimated systematic error of 20 out of 1240 channels, i.e. 0.2%.

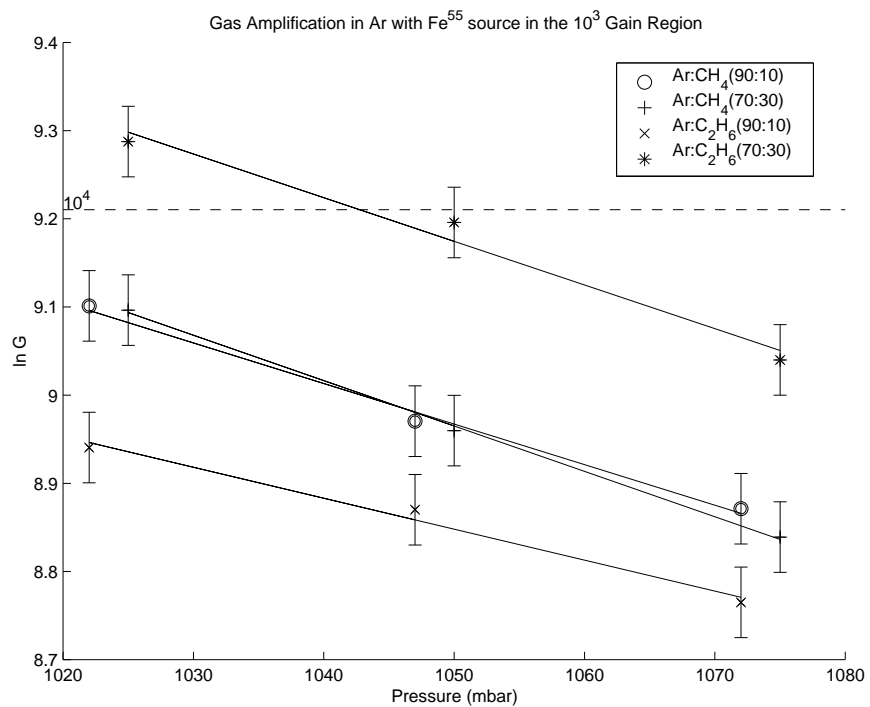


Figure 2-9: Measurements Gain v. Pressure for Ar with and  $Fe^{55}$  source.

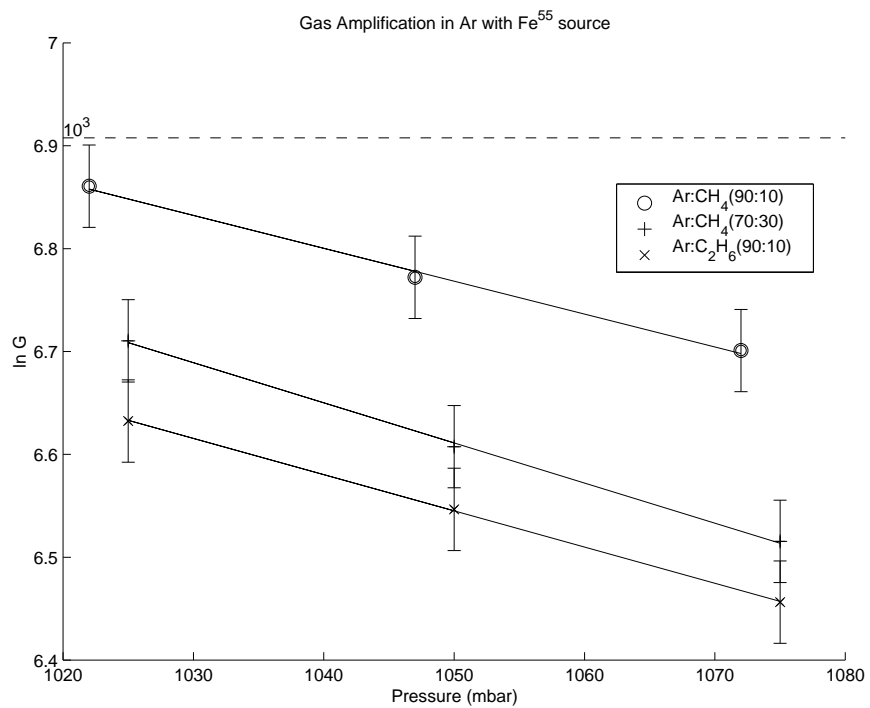


Figure 2-10: Measurements Gain v. Pressure for Ar with and  $Fe^{55}$  source.

Table 2.4: Measurements of Diethorn Parameters in Noble Gases

GAS	%	$\Delta V$	$E_{min}$
Ne:CH <sub>4</sub>	(90 : 10)	37.3 ± 5.1	16.3 ± 7.7
Ne:CH <sub>4</sub>	(70 : 30)	36.9 ± 3.8	18.2 ± 6.7
Ne:C <sub>2</sub> H <sub>6</sub>	(90 : 10)	34.4 ± 5.2	7.0 ± 3.4
Ne:C <sub>2</sub> H <sub>6</sub>	(70 : 30)	33.2 ± 3.9	23.9 ± 9.1
Ar:CH <sub>4</sub>	(90 : 10)	27.7 ± 2.5	18.6 ± 5.8
Ar:CH <sub>4</sub>	(70 : 30)	31.7 ± 1.8	41.1 ± 7.1
Ar:C <sub>2</sub> H <sub>6</sub>	(90 : 10)	30.9 ± 3.2	12.3 ± 4.7
Ar:C <sub>2</sub> H <sub>6</sub>	(70 : 30)	29.9 ± 2.0	39.7 ± 7.9
Kr:CH <sub>4</sub>	(90 : 10)	29.7 ± 3.1	36.5 ± 10.0
Kr:CH <sub>4</sub>	(80 : 20)	32.1 ± 3.2	39.2 ± 10.7
Kr:CH <sub>4</sub>	(70 : 30)	31.5 ± 2.6	47.5 ± 11.3
Kr:CH <sub>4</sub>	(60 : 40)	33.9 ± 2.8	44.5 ± 11.4
Kr:C <sub>2</sub> H <sub>6</sub>	(90 : 10)	33.1 ± 3.5	24.1 ± 8.0
Xe:CO <sub>2</sub>	(80 : 20)	31.3 ± 2.5	48.2 ± 10.1
Xe:CF <sub>4</sub>	(90 : 10)	30.3 ± 1.8	36.6 ± 6.3
Xe:CF <sub>4</sub>	(80 : 20)	27.0 ± 1.7	58.8 ± 9.8

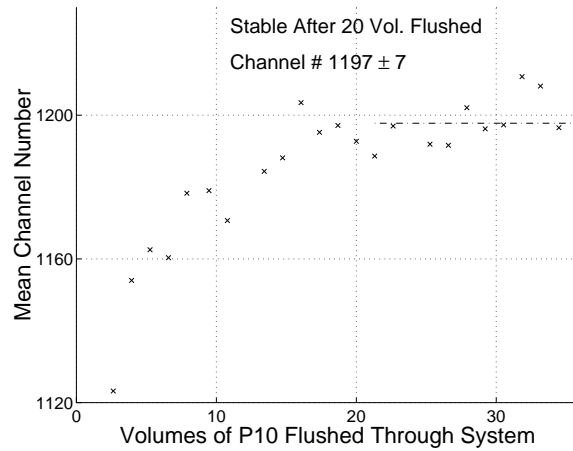
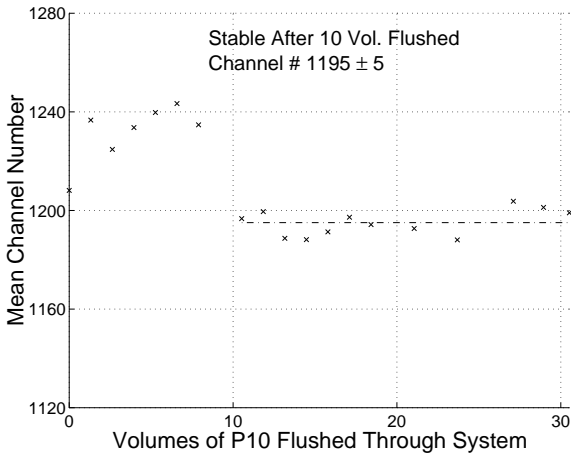
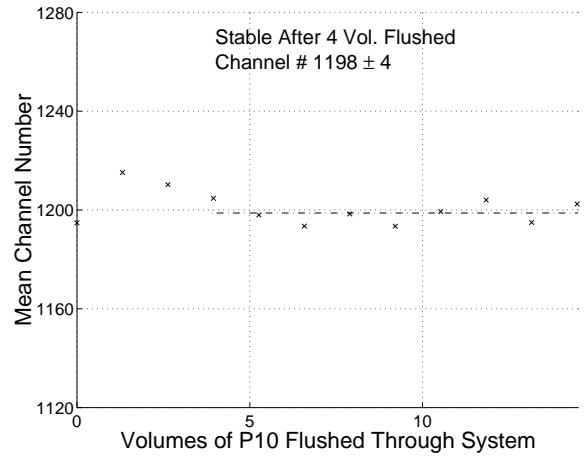


Figure 2-11: Setup time.



(a) Stability after 1 day.



(b) Electronic stability.

Figure 2-12: Stability Measurements.

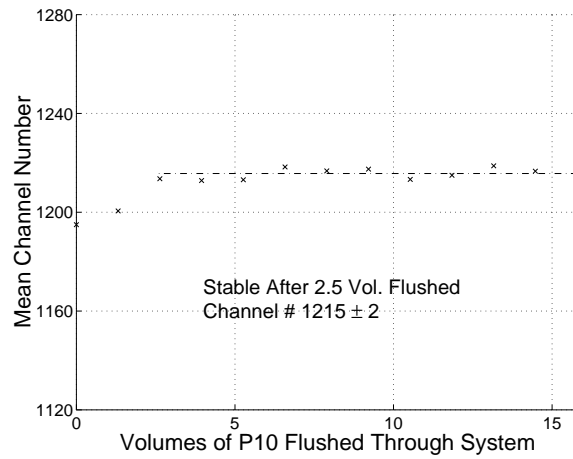


Figure 2-13: Long term stability.

# Chapter 3

## GEM Amplification Measurements

A setup was constructed to study the amplification of the GEM foils for a variety of noble gases with hydrocarbon quenchers. Different GEM geometries were studied. The amplification is dependent on the hole size: small holes offer high electric fields, but saturation is possible due to the small volume; large holes do not saturate, but offer lower electric fields. The setup for this portion of the thesis will consist of a mounted radioactive source for ionization, a drift region, exchangeable GEM foils and a wire detector to give signals at low GEM amplification.

### 3.1 Apparatus

#### 3.1.1 GEM Foils

The GEM foils are measured with an optical microscope with various illumination configurations. The hole size is measured by comparison with an etched grating with spacings of 1000 lpi. Figure 3-1 shows examples of GEM foils and Figure 3-2 shows measurements of hole sizes. Illumination from above allows measurement of the copper holes, and illumination from below allows measurement of the kapton holes. The grating (Fig 3-2) and the holes cannot be in focus at the same time, so multiple exposures must be used. The two GEMs used were the "large" foil with copper and kapton holes of radius  $190 \pm 13\mu m$  and the foil with "medium" holes of copper with

radius  $76 \pm 13\mu m$  and kapton with radius  $51 \pm 13\mu m$ .

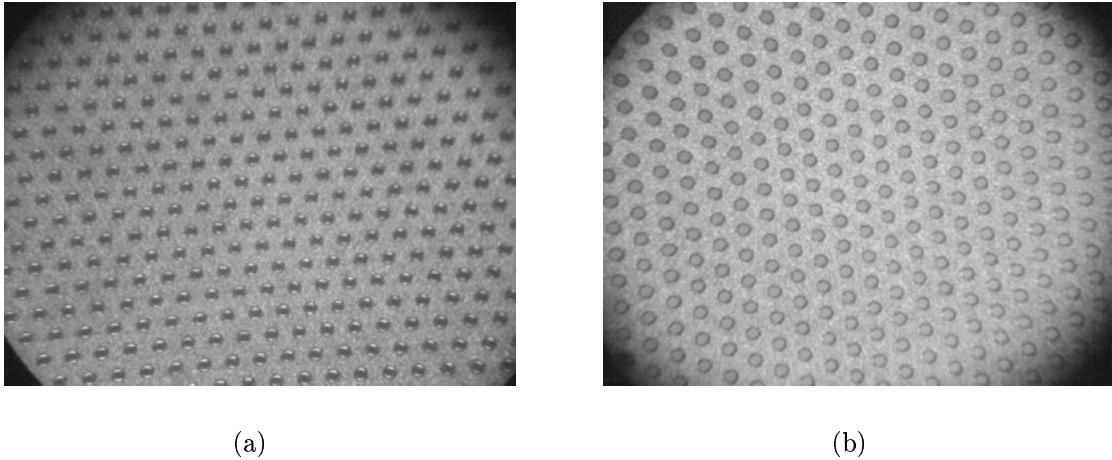


Figure 3-1: a) Medium GEM foil illuminated from below and b) from above.

### 3.1.2 Chamber Construction

With 1 mm spacing, flatness of the foils is essential for accuracy in results. To this end, the foils must be stretched to remove as many imperfections as possible. The foils are stretched with aluminum rings coated with double sided adhesive tape. The stretching occurs as a result of a differential temperature gradient between the rings and the kapton foils.

The kapton foil (including the portion with the GEM) is heated on a thick, flat aluminum plate over a hot plate. At the same time an aluminum ring, coated with tape, is cooled in a liquid nitrogen bath. The cooled ring is placed on the kapton foil, tape side down, and allowed to heat until the tape adheres to the foil. At this point, the foil is firmly attached by pressing it to the ring. This method allows tensions to be obtained on the order of  $100 \text{ N/cm}^2$ .

Once the foils are uniformly stretched, they are permanently fixed with epoxy to the smaller chamber frames. The frames have an opening of 5x5 cm and a thickness of 0.7 mm G10, and fit within the aluminum rings, as shown in Figure 3-4.

The GEM foil, cathode, and wire plate are mounted to the lid of the chamber box with use of screw presses and alignment pins (Figs. 3-5(a) and 3-7). The box

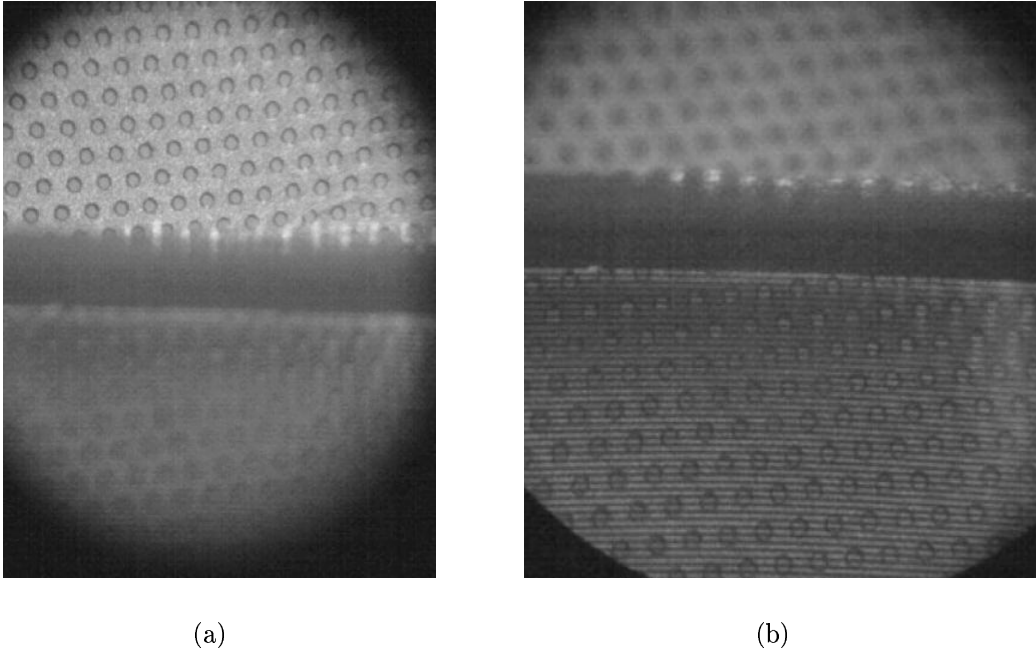


Figure 3-2: a) Medium GEM foil with grating, holes are in focus. b) Same foil, but grating is in focus.

has been leak tested by fully immersing the sealed chamber in water and filling to approximately 90 psi with P10.

A schematic of the circuit used to supply the high voltage to the wires can be seen in figure 3-5(b).

### 3.1.3 First GEM Experiment

A GEM foil with large holes  $190 \pm 13\mu m$  was used first for measurements. Several foils were stretched and assembled in the chamber, and attempts were made at taking data with them. Under moderate operating conditions, there was sparking observed in the foils which shorted out the GEM foils. The circuit used was not current limited, so even if the power was manually turned off to the GEM foil immediately, the GEMs were rendered unusable. They did not recover when cleaned with an ultrasonic bath.

Microscopic analysis showed (Fig. 3-8) that the batch of GEM foils with large holes that were incorrectly fabricated. The holes were etched straight through rather than beveled. The holes, when cut at a bevel, can support a potential difference,

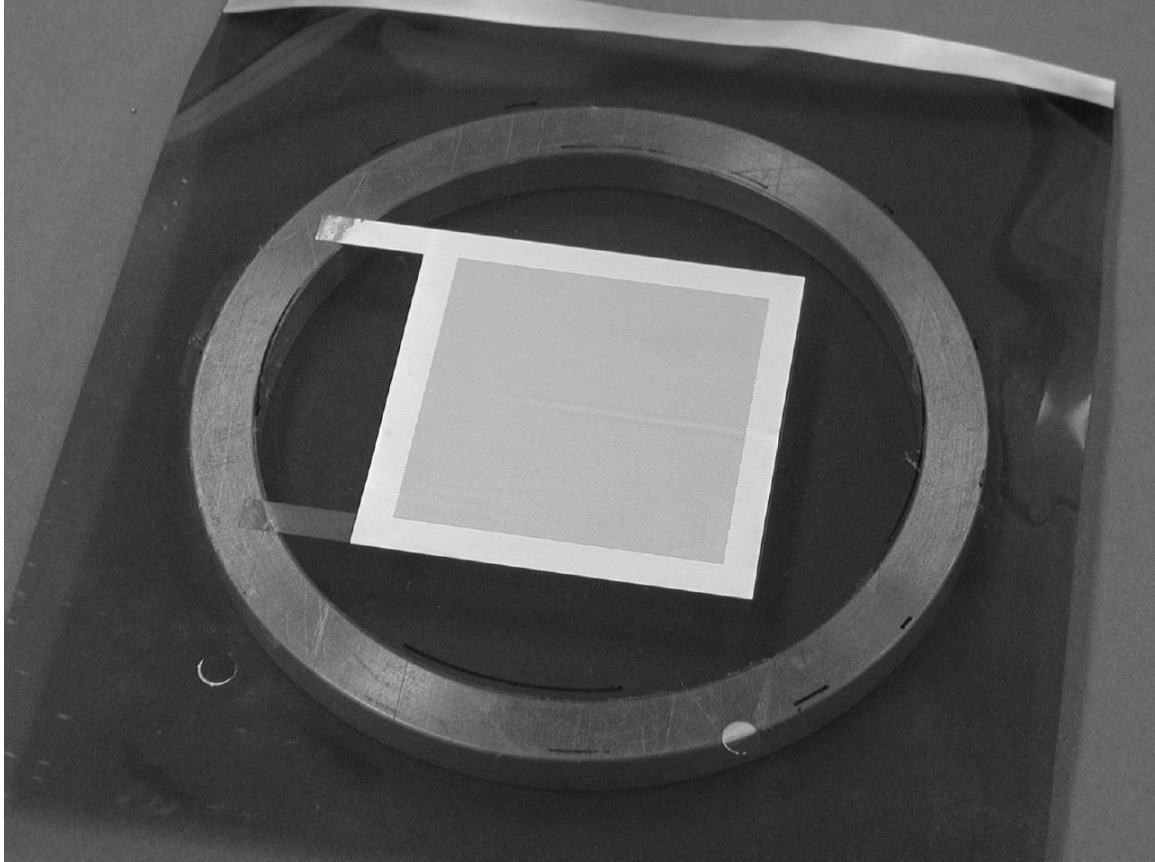


Figure 3-3: Gem stretched on Aluminum ring.

but when cut straight through, are prone to sparking, and cannot be taken to the necessary potentials of 300 – 400V. These foils are unusable.

The batch of foils with "medium size" holes of  $76 \pm 13\mu m$  for the copper hole, and  $51 \pm 13\mu m$  for the kapton hole, showed a correctly beveled edge on the hole and were used in the following sections. This cut can be seen in figure 3-1, with different lighting sources two hole diameters can be observed.

## 3.2 Measurements

The product of the amplification factor of the GEM and the electron transfer through the foil is defined as the ratio of the signal at a certain GEM voltage compared to that of  $V_{GEM} = 0$ . This amplification factor is measured as a function of GEM voltage, transfer field, and drift field.



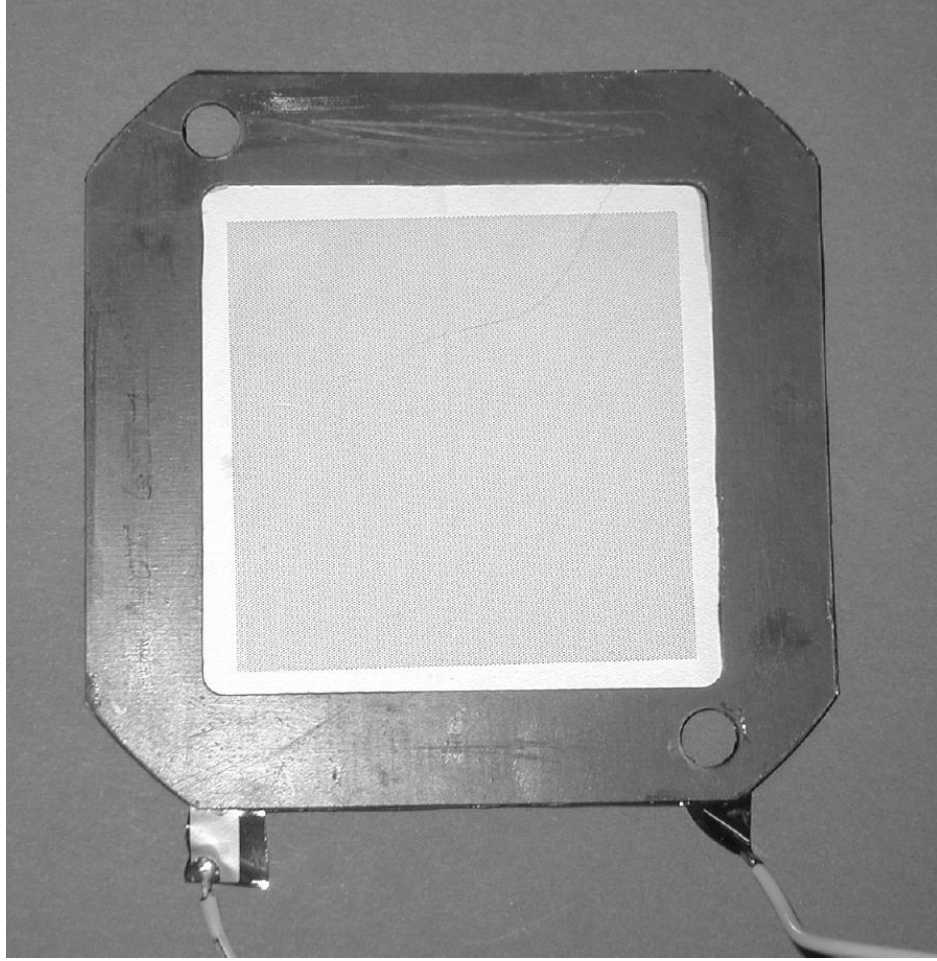


Figure 3-4: Gem foil mounted on G10 frame.

### 3.2.1 Measurements

The  $5.9keV\gamma$  from  $Fe^{55}$  will be stopped in the foreseen gas volume of depth  $d$  (Fig. 3-9) with 70% probability in the gas, making a deposit of approximately 200 electrons, 8% of the electrons penetrate through the GEM foil and create full signals in the amplification volume of depth  $s$ . These signals calibrate the wire gain  $G_0$ . Events in volume  $d$  have their ionization drifted through the GEM with an average fraction  $T(V_{GEM})$  transmitted into the amplification region, so that the measured gain is

$$G_{Tot} = T(V_{GEM}) \times G_{GEM} \times G_0 \quad (3.1)$$

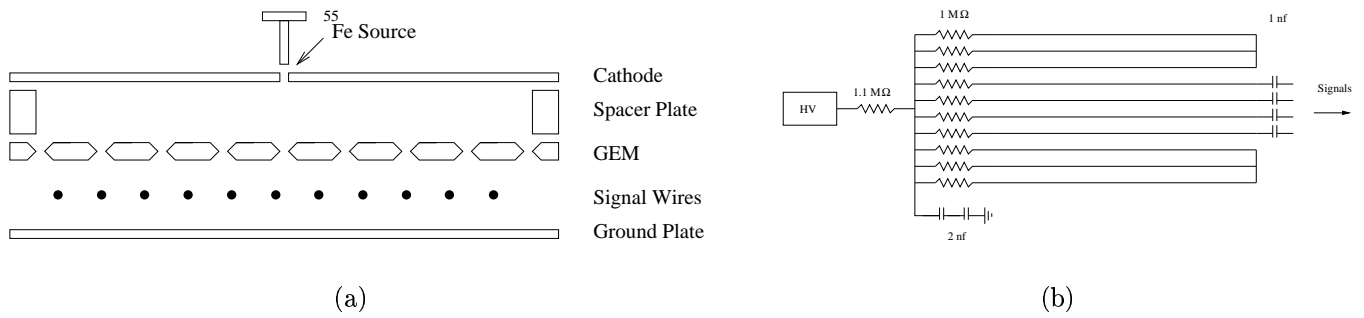


Figure 3-5: Schematic Diagrams for a) GEM chamber and b) wire circuit.

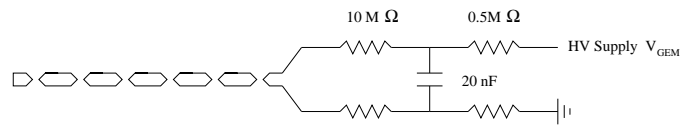


Figure 3-6: Circuit connecting GEM foil.

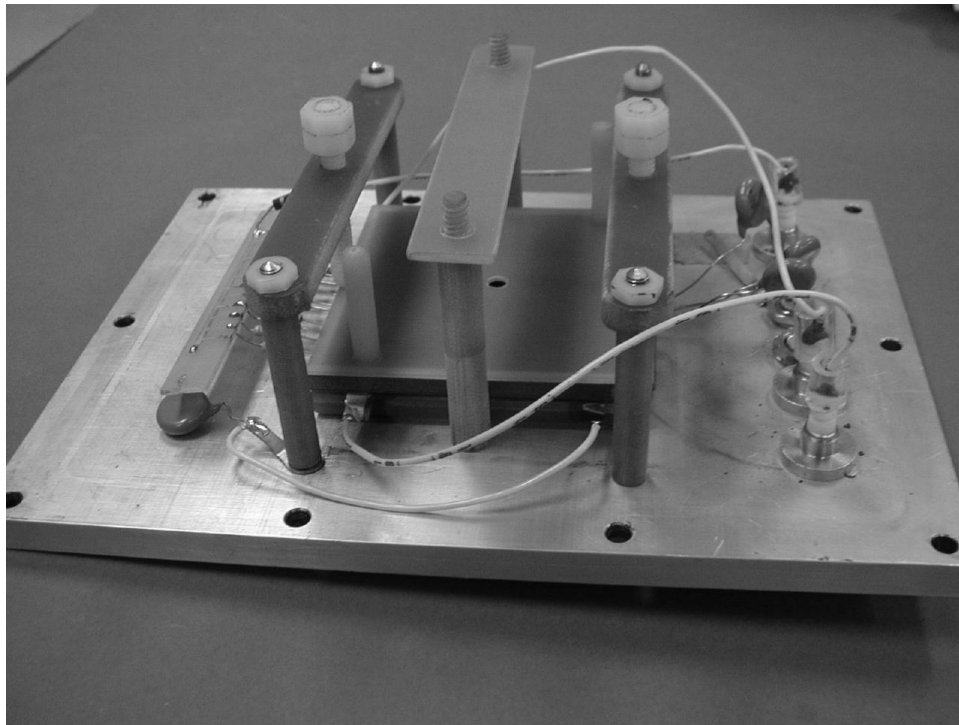
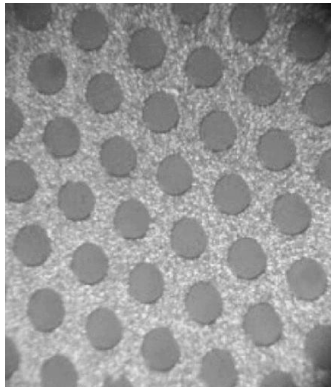
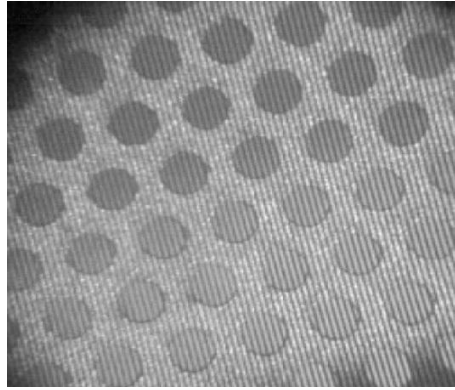


Figure 3-7: Assembled chamber complete with circuit elements.



(a)



(b)

Figure 3-8: a) GEM foil with large holes illuminated from above and b) with grating.

### 3.2.2 Single GEM

The configuration for the single GEM measurements is shown in Figure 3-9. Figure 3-10(a) shows a histogram dominated by the spectrum of calibration signals of  $\text{Fe}^{55}$  in the signal wire setup. The data in the histogram is the unnormalized charge measurement from the integration of the negative pulse on the signal wires. For  $V_{GEM} \leq 100V$ , obviously the ionization is not properly transferred, and  $T(V_{GEM}) \cdot G_{GEM} \leq 0.5$ . With increasing  $V_{GEM}$ , the signals from volume  $d$  gradually overtake the calibration peak and grow to large values.

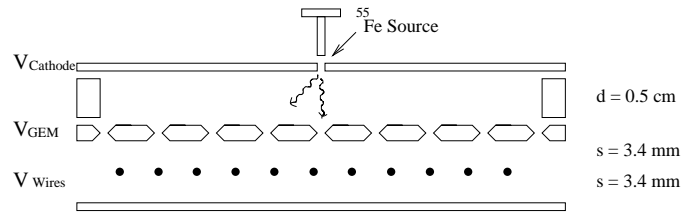
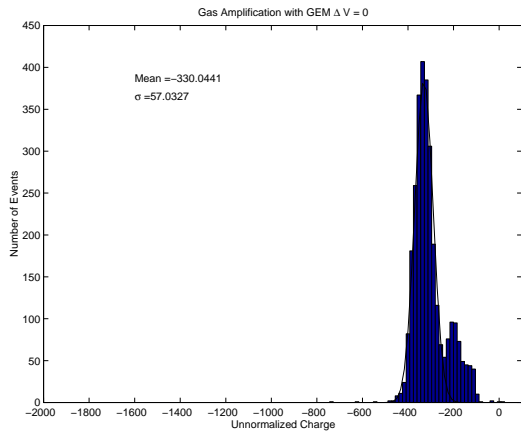
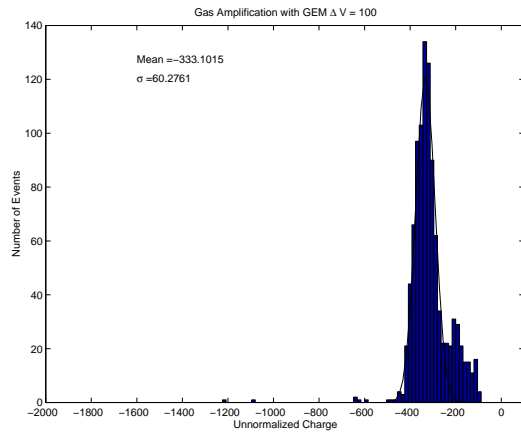


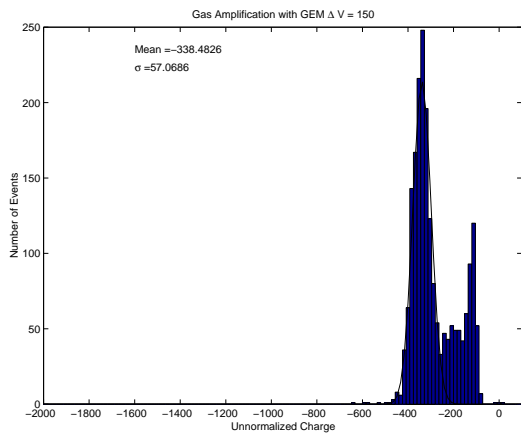
Figure 3-9: GEM chamber schematic for a single foil.



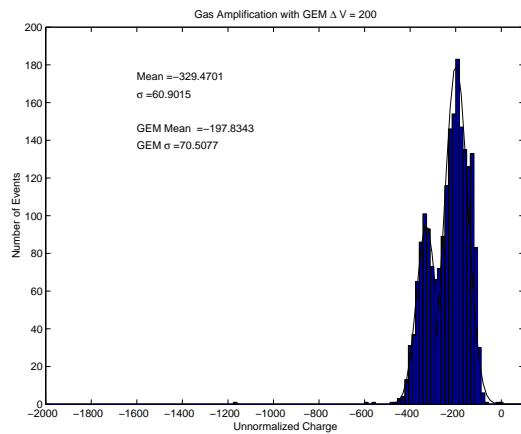
(a)  $V_{GEM}=0$



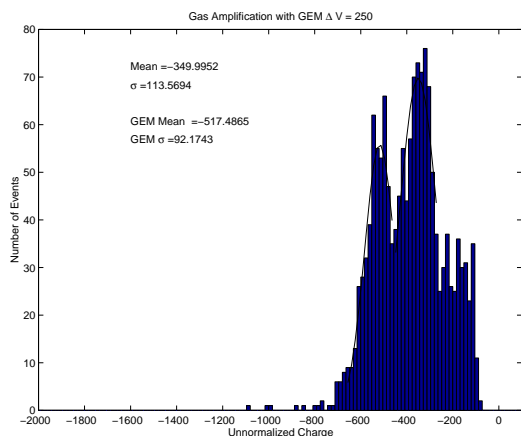
(b)  $V_{GEM}=100$



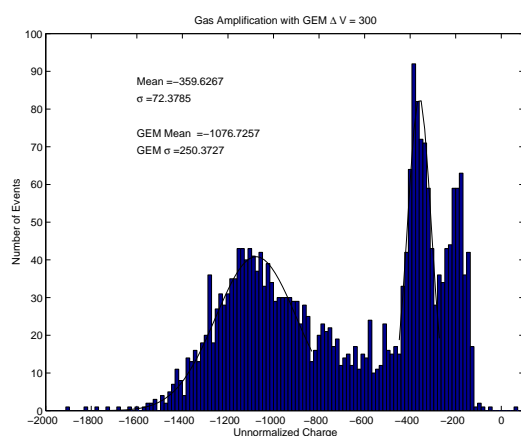
(c)  $V_{GEM}=150$



(d)  $V_{GEM}=200$

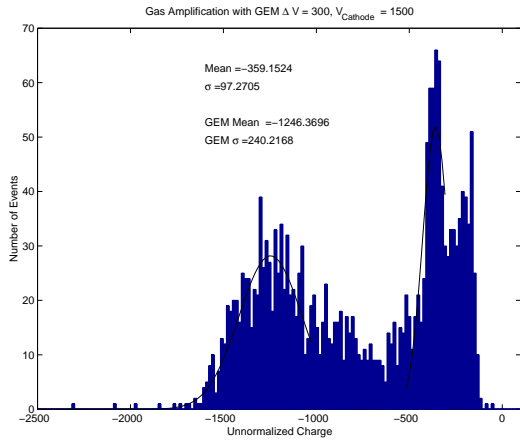


(e)  $V_{GEM}=250$

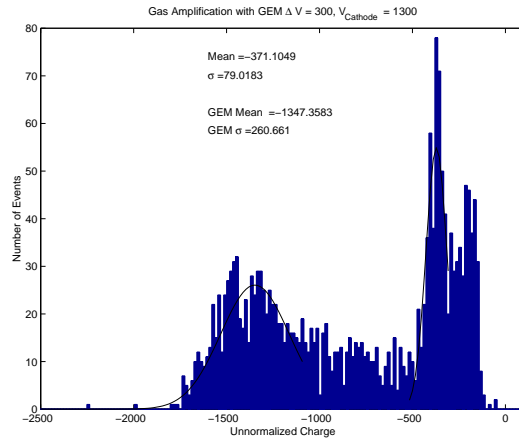


(f)  $V_{GEM}=300$

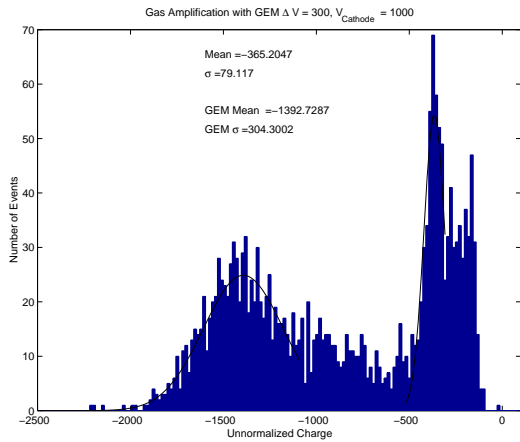
Figure 3-10: Signal charge distribution from a  $5.9keV\gamma$  ionization in P10. The peak at channel  $-330$  corresponds to the calibration signals with  $V_{wire} = 1600V$ . The other peaks are gradually GEM amplified signals.



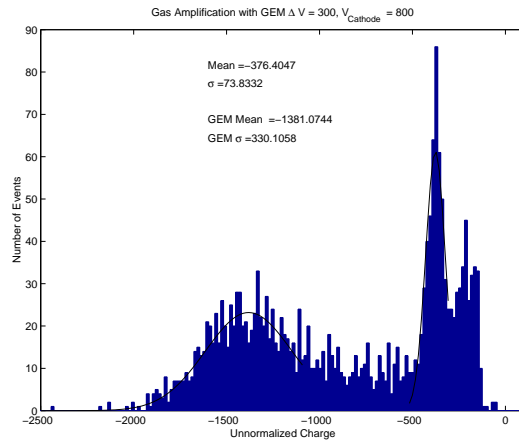
(a)  $V_{GEM}=300$  Cathode Voltage = 1500



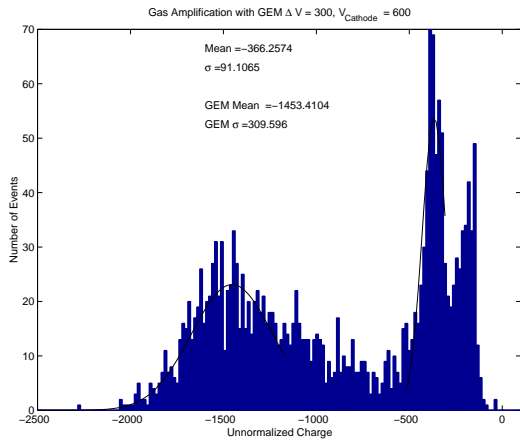
(b)  $V_{GEM}=300$  Cathode Voltage = 1300



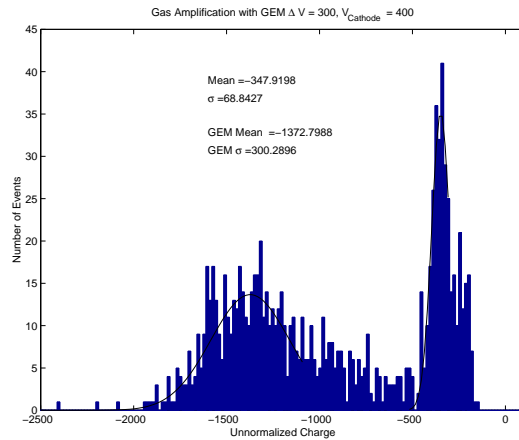
(c)  $V_{GEM}=300$  Cathode Voltage = 1000



(d)  $V_{GEM}=300$  Cathode Voltage = 800



(e)  $V_{GEM}=300$  Cathode Voltage = 600



(f)  $V_{GEM}=300$  Cathode Voltage = 400

Figure 3-11: Signal charge distribution from a  $5.9\text{keV}\gamma$  ionization in P10. The peak at channel  $-330$  corresponds to the calibration signals with  $V_{\text{wire}} = 1600\text{V}$ . The GEM amplified signals (near channel  $-1400$ ) show little dependence on the drift field in volume  $d$ .

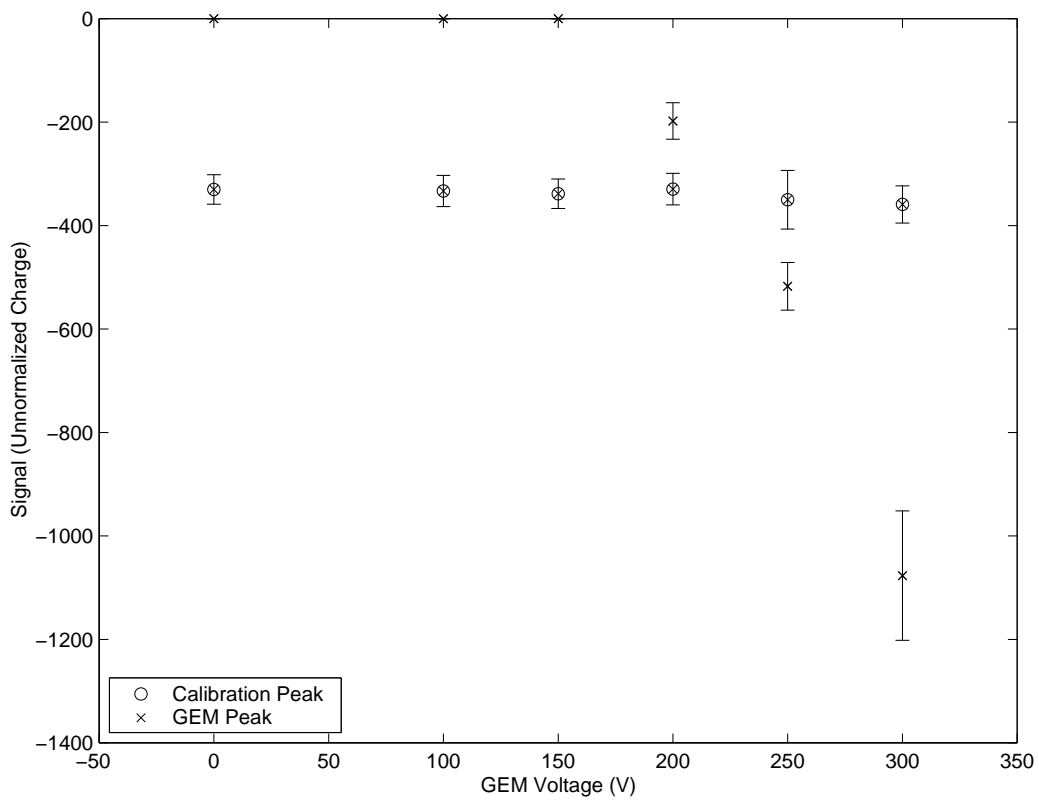


Figure 3-12: Signal v. Gem Voltage for Single GEM chamber.

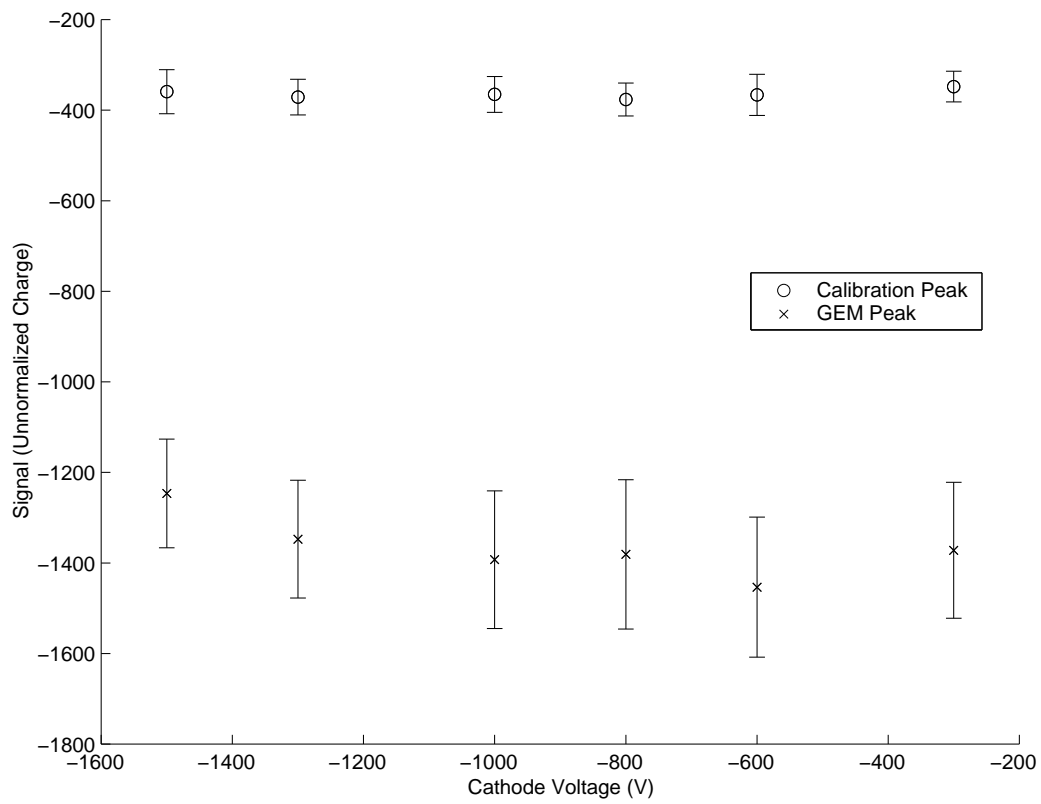


Figure 3-13: Signal v. Cathode Voltage for Single GEM chamber.



### 3.2.3 Double GEM

An additional GEM with medium sized holes was stretched and placed in the chamber. The two foils are spaced  $0.7\text{mm}$  apart. Figure 3-14 shows the circuit providing voltage to the two foils, in fact  $V_{G1} = V_{G2} = V_T$ . An  $\text{Am}^{241}$  source ( $5\text{MeV}\alpha$ ) was mounted instead of the  $\text{Fe}^{55}$ .

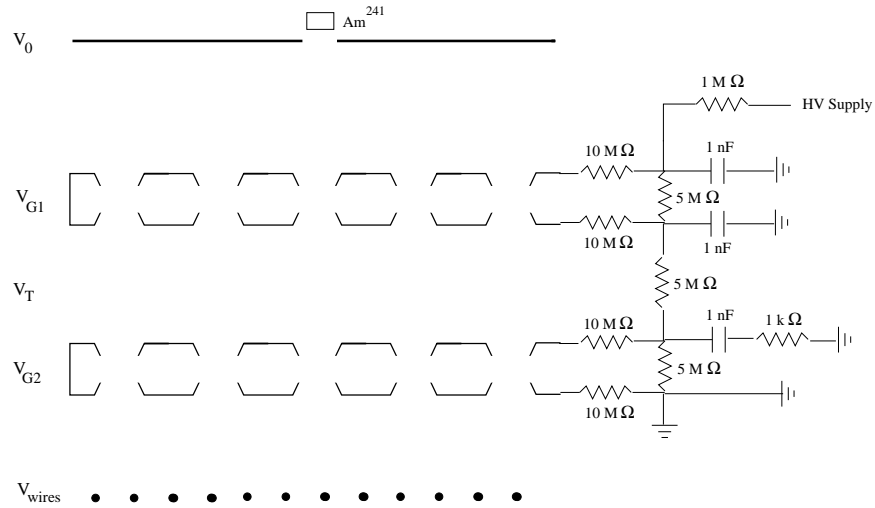


Figure 3-14: Circuit connecting two GEM foils.

This is a first measurement with a double GEM chamber using  $\text{Ar:DME}(50 : 50)$ . Results are shown in Figure 3-15. The cathode was set so that there was an ample drift field between the source and GEM, approximately  $200 - 600\text{V/cm}$ . The wire voltage of  $1410\text{V}$  provided a constant calibration signal of  $8\text{mV}$  for  $\alpha$  particles directly penetrating into the wire gap.

Figure 3-15 shows these control calibration signals as a dashed line. The amplified signals were observed in a noble way: no signals when the drift field was reversed, clear signals when the drift field directs the ionization toward the GEM foils. Where as it was shown before that the transfer from the ionization volume to the first GEM is almost independent of  $V_d$ , the transfer between the GEMs depends on  $V_T (= V_{G1} = V_{G2}$  here).

Also, the transfer field from the last GEM to the wires could not be varied and may be  $\ll 100\%$ , due to electrons terminating on the lower GEM plate rather than on the wire. Due to the electric circuit used, we expect

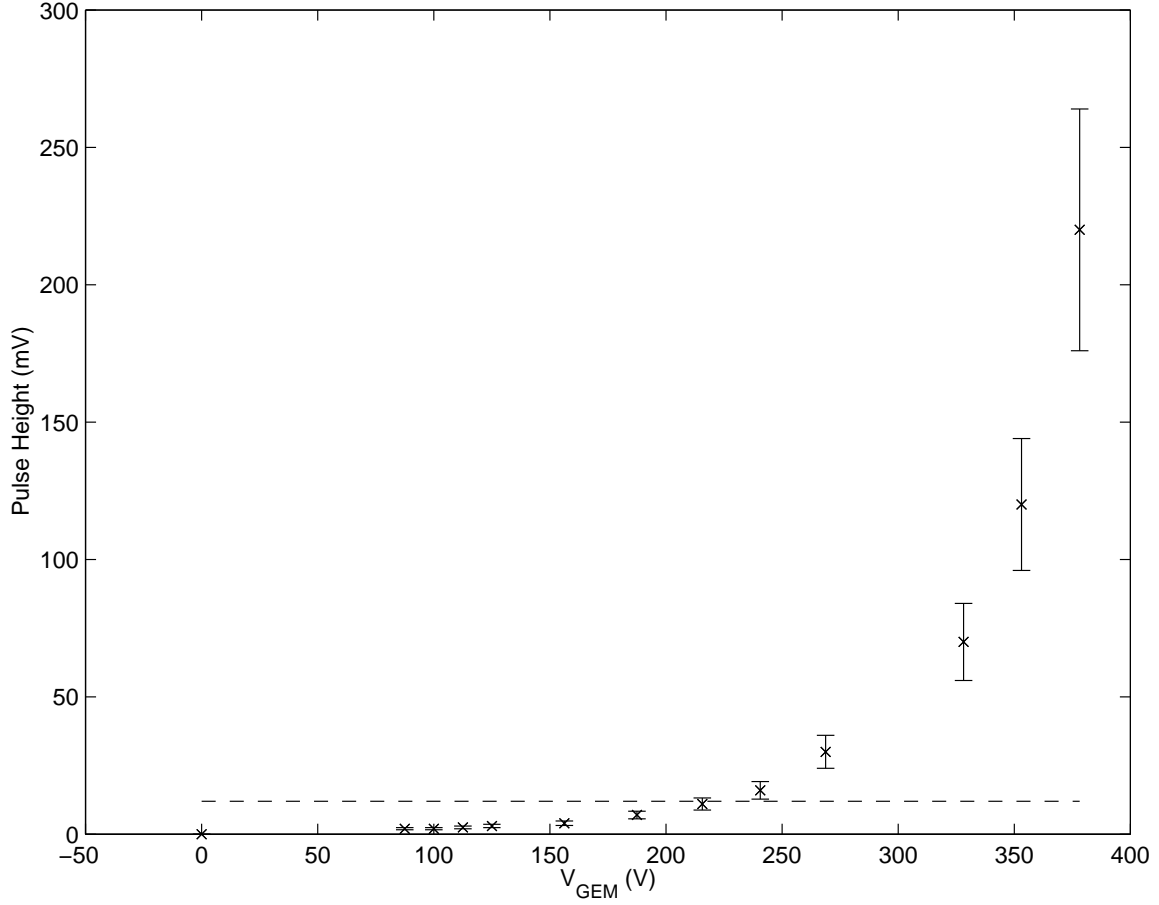


Figure 3-15: Pulse height for double GEM v.  $V_{G1} = V_{G2}$ .

$$Pulseheight \propto G_0 \cdot G_{G^2} \cdot T_{GEM} \cdot T_{GEM-wires} < G_G^2. \quad (3.2)$$

From the smallest to largest signals obtained, we find 100-200x amplification. With further optimization of transfer fields these double GEMs are ideal for TPCs in NLC (or TESLA).

# Chapter 4

## Summary

A systematic study of gas multiplication, gain, for four noble gases, 16 mixtures, has been done. Differential measurements with respect to voltage and pressure, as well as absolute gain measurements, are presented. Along with this data, the Diethorn parameters,  $E_{min}$  and  $\Delta V$  have been extracted. Further measurements will involve a larger range of pressure measurements to lessen the correlation between the Diethorn [1] parameters.

A GEM chamber was constructed to study various chamber geometries. First results on single and double GEM are also presented. With the double GEM chamber, an estimated amplification factor of 100-200 has been achieved. In the future, further elimination of wires is proposed, with alternatives to a wire readout plane as well as further optimization of the transfer fields between chamber elements.



# Bibliography

- [1] W. Diethorn. A methane proportional counter system for natural radiocarbon measurements. USAEC Report NY06628, 1956. also doctoral dissertation, Carnegie Inst. of Technology.
- [2] A.V. Engel. Ionization in gases by electrons in electric fields. Handbuch der Physik, ed. S. Fluegge, 1956. as cited in W. Blum and L. Rolandi. Particle Detection with Drift Chambers, Springer-Verlag, 1994.
- [3] U. Fano. *Annual Review of Nuclear Science*, volume 13, pages 1+. 1963.
- [4] W. R. Leo. *Techniques for Nuclear and Particle Physics Experiments*, chapter 6. Springer-Verlag, 1987.
- [5] MAXWELL 3D FIELD SIMULATOR version 1.9.04 (1984-1997) - program for creating the field maps used for the simulation by Ansoft Corporation.